

W001

Reducing Uncertainties in Anisotropic Tomography

J. Cai (TGS-NOPEC Geophysical Company), Y. He (TGS) & L. Geiger* (TGS)

SUMMARY

One of the fundamental challenges for anisotropic tomography is the trade-off between the inverted velocity correction and the anisotropic parameters correction. The studies in this paper find that the conventional tomography solution is not sufficient to resolve the updates in velocity and in the anisotropic parameters. The tomography solver needs to be modified to include additional precondition, such as geological and well constraints for inversion, in order to reduce the uncertainties and provide geologically consistent anisotropic models.

Introduction

In order to improve the subsurface image accuracy, anisotropic imaging, both Tilted Transverse Isotropic (TTI) and Vertical Transverse Isotropic (VTI), has become routine in seismic processing. However, the anisotropic model building and workflows are still challenging.

Tomography as a velocity model building tool has been studied and used in processing (Wang et al., 1995). Anisotropic tomography was also used to estimate anisotropic parameters and to build anisotropic models (Yuan et al., 2006 for 3D VTI; Zhou et al., 2004 for 2.5D TTI).

We have developed an anisotropic tomography technique to simultaneously invert both the velocity and anisotropic parameters (He and Cai, 2011). In this paper, we will address how to solve the trade-off between the velocity and the anisotropic parameters from inversion.

Focusing Analysis (FAN) for VTI and TTI anisotropic estimates at well locations was developed in 2008 and has since been used in our anisotropic PSDM projects (Cai et al., 2009). The key for the FAN technique is using check shot information to separate the velocity contributions from the anisotropic parameters. Consequently, FAN can be used to provide the tomography with initial anisotropic models which are close to the global minimum, and tomography can further refine them. Tomography provides a linearized solution to a nonlinear problem. This normally requires the initial model for tomography to be close to the true model (residual of the travel time is at the global minimum) in order to avoid being trapped in a local minimum. In this study, we try to combine the strengths of both FAN and tomography, to provide a practical solution for anisotropic model building.

Anisotropic tomography and its challenges

A general description of anisotropic media includes five parameters: velocity, two Thomsen's anisotropic parameters (ϵ and δ), and the anisotropic symmetry axis' tilted angle and azimuth. A previous study (Audebert and Dirks, 2006) indicates that the decoupling of the anisotropic parameters is greatly simplified by assuming that the tilted anisotropic axis coincides with the dip of the structure. In this study, we assume the tilted axis is perpendicular to the structure dip. In turn the anisotropic parameters are reduced to velocity and two Thomsen's parameters.

Simultaneous inversion anisotropic tomography can be described by solving the linear system,

$$\begin{bmatrix} \frac{\partial t}{\partial v_o} & \frac{\partial t}{\partial \delta} & \frac{\partial t}{\partial \epsilon} \end{bmatrix} \begin{bmatrix} \Delta s_o \\ \Delta \delta \\ \Delta \epsilon \end{bmatrix} = r \quad (1)$$

where s_o is the slowness of v_o velocity, ϵ and δ are Thomsen's parameters, and r is the vector of the travel time residuals. Because the size of this linear system is larger, normally Equation 1 is solved by using a conjugate gradient algorithm. Regularization could be added to improve the solution stability,

$$w_v L_v \Delta s_o = 0; w_a L_a \Delta \delta = 0; w_a L_a \Delta \epsilon = 0 \quad (2)$$

where L_v is the slowness regularization term; w_v is the weight for slowness regularization. L_a is the anisotropic parameter regularization term; w_a is the weight for anisotropic regularization.

To gain more insight, we studied a simple model containing ten horizontal layers, and solved Equations 1 and 2 by the singular value decomposition method. Figure 1 shows the resolution matrix (Figure 1a) and the covariance matrix (Figure 1b). In Figure 1a, A, B, and C are the resolution matrices for Δs_o , $\Delta \delta$, and $\Delta \epsilon$, respectively. The resolution matrices indicated that for the same ray path, the slowness is more likely to be resolved, ϵ is the least likely to be resolved, and δ is in between. In the covariance matrix (Figure 1b), the diagonal elements in sub-matrix A correspond to Δs_o , the diagonal elements in sub-matrix B correspond to the unknown $\Delta \delta$, and the diagonal elements in sub-

matrix C correspond to the unknown $\Delta\varepsilon$. We can see that there is a strong interdependence between the velocity and the anisotropic parameters (diagonal elements in sub-matrices AB and AC). There is also strong interdependence between the two anisotropic parameters (diagonal elements in sub-matrices BC).

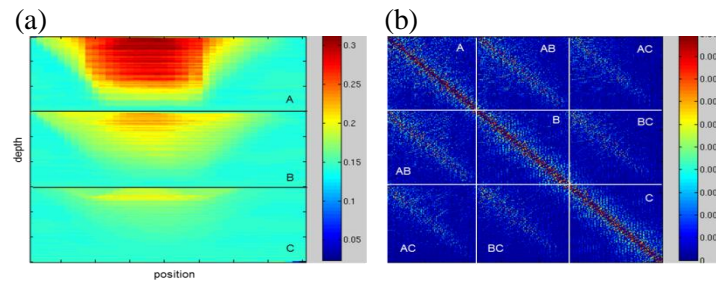


Figure 1: Resolution matrices (a) and covariance matrices (b) for a simple model with ten horizontal layers.

Consequently, in practice, it is preferred to use the check shots if they are available, to help separate the velocity contributions from the anisotropic parameters. The check shot constraints can be described as constraining the check shot travel time,

$$C(v_0, \varepsilon, \delta) = t_c \quad (3)$$

where t_c is the check shot time.

To validate the algorithm, the BP 2008 TTI benchmark model was used. The velocity perturbation (Figure 2b) was added to the true velocity model (Figure 2a) to generate the initial velocity model. One check shot was generated for testing.

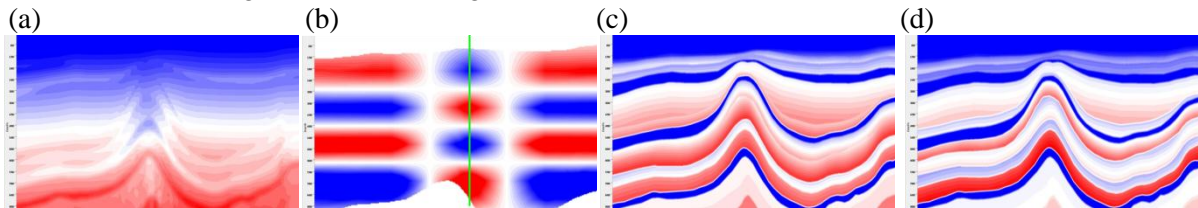


Figure 2: True velocity model (a) and velocity perturbation (b). One check shot (location of green line) is used. (c) and (d) are the true δ and ε models, respectively. True models courtesy of BP.

Figure 3 shows the first iteration tomography inversion results for Equation 1 with the regularization (Equation 2) and check shot constraints (Equation 3) applied. Some hints of these updates can be seen in the updated models, but overall the results are far from the actual models (Figures 2b and 2c).

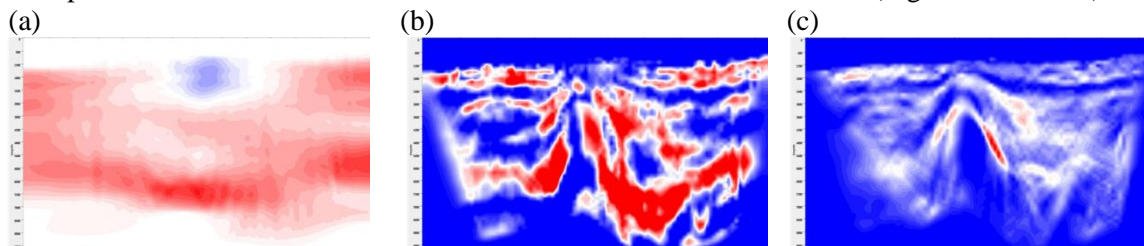


Figure 3: Tomography with regularization solution for velocity correction (a), δ (b) and ε (c) models.

To further improve the algorithm, a precondition was introduced to modify the tomography Equation 1 to

$$\begin{bmatrix} \frac{\partial t}{\partial v_0} & \frac{\partial t}{\partial \delta} & \frac{\partial t}{\partial \varepsilon} \end{bmatrix} \begin{bmatrix} I & p_a & p_a \end{bmatrix} \begin{bmatrix} \Delta s_0 \\ \Delta \delta \\ \Delta \varepsilon \end{bmatrix} = r \quad (4)$$

where I is the identity matrix, and p_a is the precondition term for the anisotropic parameters, ε and δ . In the precondition term, we combined certain geological knowledge, such as the assumptions that

anisotropy generally follows structure, the wavelength for anisotropy normally is very low, and generally they are much smoother than the velocity variation, etc.

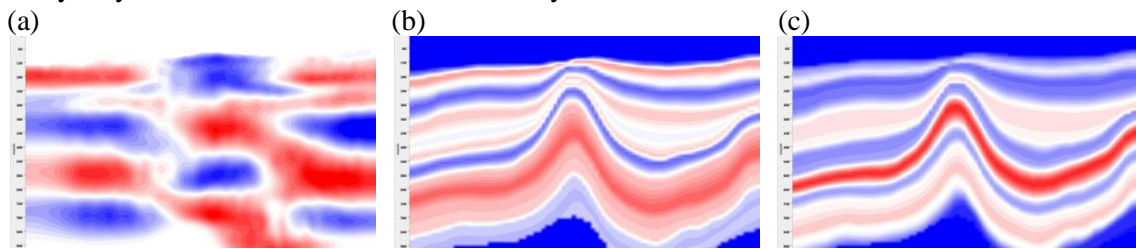


Figure 4: The third iteration results for preconditioned tomography solution with one check shot for velocity correction (a), δ (b) and ϵ (c) models.

The third iteration results from Equation 4 are shown in Figure 4. Compared to the simple regularization results (Figure 3), it shows that the anisotropic models conform to the structure well and are closer to the true anisotropic models (Figures 2c and 2d). The precondition results were able to recover the negative velocity correction trend in the middle, which was missed in the regularization result. The common image gathers (CIGs) (Figure 5) show that the inverted models improve the flatness of the CIGs. By adding the correct structure precondition for anisotropy, we implicitly reduce the unknown's freedom. In the shallow part, because of the wide reflection angle coverage, there is better separation between the contribution from the velocity and the anisotropic parameters. In turn, the inversion results converge better for the shallow part compared to the deep part. Because there is a lack of reflection angle resolution in the deeper section, in practice, we normally dampen the anisotropic parameters gradually to a small constant varying with depth.

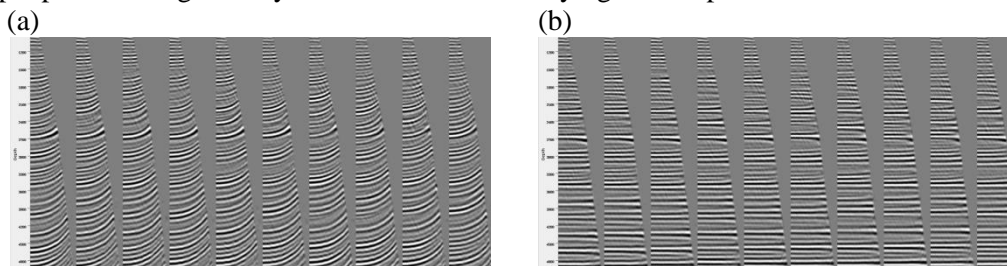


Figure 5: CIGs for initial isotropic migration (a); CIGs from anisotropic tomography update from Equation 4 (b).

Field data examples

TTI anisotropic tomography was used on data from TGS' Kepler WAZ survey in Gulf of Mexico. The initial anisotropic model was built from check shots. Firstly, FAN was applied at each check shot location; followed by horizon-guided interpolation to build the smooth anisotropic model. Anisotropic migration was used to generate the CIGs. Next, simultaneous anisotropic tomography was used to derive the velocity, epsilon and delta, while check shots were used as constraints.

The anisotropic tomography derived models (Figure 6) effectively flatten the CIGs (Figure 7b compares to Figure 7a); in turn, improving the stack images (Figure 7d compares to Figure 7c).

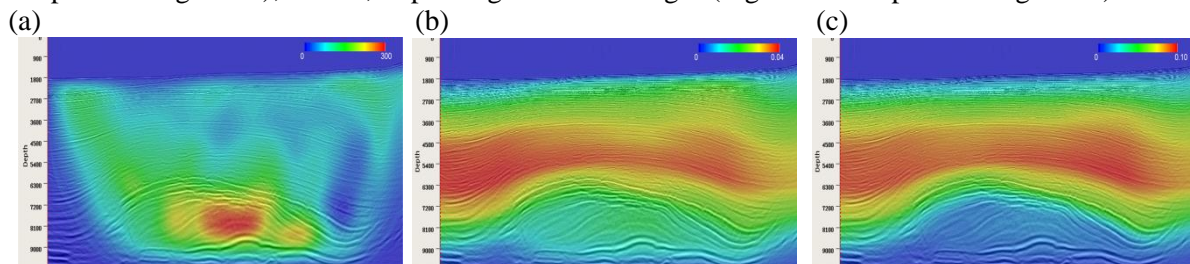


Figure 6: Anisotropic tomography inverted models, velocity correction (a), δ (b) and ϵ (c).

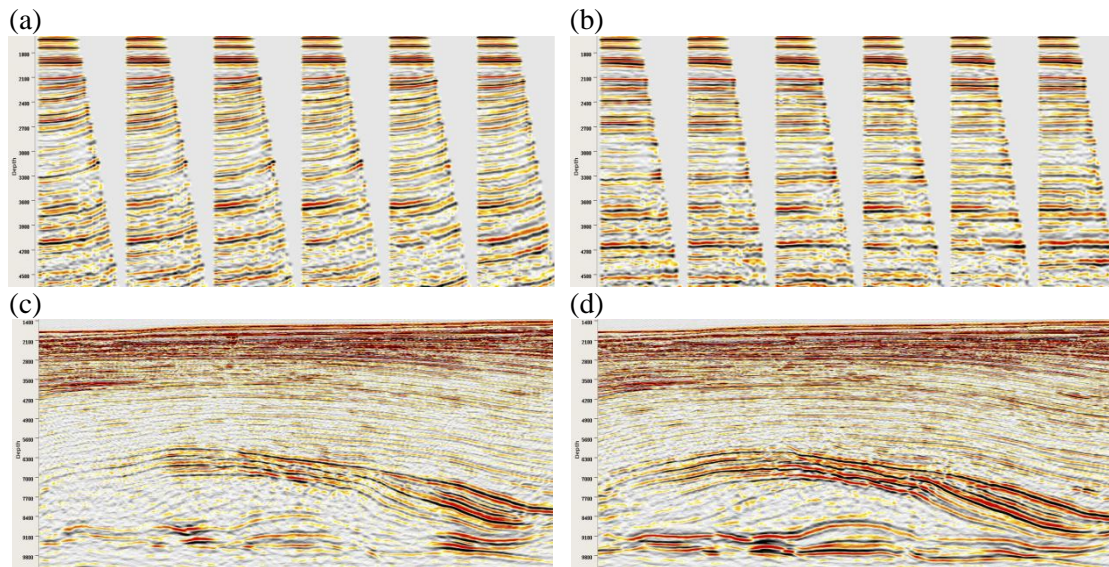


Figure 7: CIGs (a) and migration stack (c) from isotropic migration using initial model. CIGs (b) and migration stack (d) using anisotropic tomography derived models.

Conclusions

The studies in this paper show that conventional tomography regularization is not sufficient to solve the uncertainties between velocity and the anisotropic parameters. The tomography solver needs to be modified to include the precondition, which introduces geological constraints for tomography. By combining the precondition with the check shot information and starting from better initial models derived from the FAN method, the uncertainties of the anisotropic inversion can be reduced in practice.

Acknowledgements

The authors would like to thank Bin Wang and Zhiming Li for their helpful advice during this project, Laurie Geiger and Simon Baldock for proof reading. We thank the management of TGS for permission to publish this paper and BP for the initial synthetic TTI benchmark.

References

- Audebert, F. and V. Dirks, 2006, TTI Anisotropic Depth Migration: What tilt estimate should we use? SEG Expanded Abstracts, 2382-2386.
- Cai, J., Y. He, Z. Li, B. Wang, and M. Guo, 2009, TTI/VTI anisotropy parameters estimation by focusing analysis, Part I: theory, SEG Expanded Abstracts, 301-305.
- He, Y. and J. Cai, 2011, anisotropic tomography for VTI and TTI media, SEG Expanded Abstracts, 3923-3927.
- Wang, B., K. Pann, and R. A. Meek, 1995, Macro velocity model estimation through model based globally-optimized residual-curvature analysis: SEG, Expanded Abstracts, 1084-1087.
- Yuan, J., X. Ma, S. Lin, D. Lowrey, 2006, P-wave tomographic velocity updating in 3D inhomogeneous VTI media, SEG Expanded Abstracts, 3368-3372.
- Zhou, D. Pham, S. Gray, B. Wang, 2004, Tomographic velocity analysis in strong anisotropic TTI media, SEG Expanded Abstracts, 2347-2350.